Journal of Materials Chemistry C

PAPER

View Article Online
View Journal | View Issue

Cite this: J. Mater. Chem. C, 2014, 2, 8750

A UV-absorber bismuth(III)-*N*-methyldiethanolamine complex as a low-temperature precursor for bismuth-based oxide thin films†

Dulce Pérez-Mezcua,[a] Rafael Sirera,[b] Ricardo Jiménez,[a] Iñigo Bretos,[a] Christopher De Dobbelaere,[c] An Hardy,[c] Marlies K. Van Bael[c] and M. Lourdes Calzada*[a]

Received 9th May 2014
Accepted 20th August 2014

DOI: 10.1039/c4tc00960f

www.rsc.org/MaterialsC

Novel synthetic methods in solution that reduce the formation temperature of bismuth-based electronic oxides are essential for their successful integration with substrates of low thermal stability within micro- and flexible-electronic devices. This has become crucial for these oxides, since they appear as promising low-toxic functional materials alternative to other electronic oxides containing heavy metals. However, this is a challenge, since the crystallization of bismuth oxides occurs at high temperatures. To overcome these problems, we synthesize here a UV-absorber charge transfer metal complex in solution between the Bi(III) ion and an alkanolamine, *N*-methyldiethanolamine (Bi(III)–mdea). We take advantage of the photoreactivity of this complex to prepare bismuth-based oxide thin films at low temperature, which cannot be achieved by traditional thermal processing methods. Room temperature stable oxide thin films of the high-temperature δ-Bi_2O_3 phase are prepared from these solutions by UV-irradiation and annealing at 350 °C. The efficiency of this synthetic strategy is additionally proven for the low temperature preparation of thin films of much more complex bismuth based functional oxides: the multiferroic bismuth ferrite, $BiFeO_3$, and the relaxor-ferroelectric perovskite of bismuth, sodium and barium titanate, $(Bi_{0.5}Na_{0.5})_{0.945}Ba_{0.055}TiO_3$.

1. Introduction

Bismuth based materials exhibit a broad spectrum of applications ranging from non-toxic pigments (bismuth vanadate), Lewis acid catalysts (bismuth triflate), biomaterials for medicine (bismuth subsalicylate) and cosmetics (bismuth oxychloride), to thermoelectrics (bismuth telluride compounds) for electric energy convertors and ferroelectrics (bismuth based perovskites) for memory devices, sensors and actuators.[1]

Single bismuth(III) oxides show optical and electrical properties, which make them potential candidates for applications in optoelectronics, optical coatings, gas sensors or solid electrolytes.[2] Various polymorphics of Bi_2O_3 have been reported in the literature,[1] including α-Bi_2O_3, β-Bi_2O_3, γ-Bi_2O_3, δ-Bi_2O_3, ε-Bi_2O_3 and ω-Bi_2O_3, which differ significantly in their optical and electrical properties. Low-temperature α-Bi_2O_3 is a p-type semiconductor which transforms into δ-Bi_2O_3 at 729 °C. The high-temperature cubic δ-Bi_2O_3 phase is among the most effective oxide ion conductors,[3] which makes it useful in fuel cells and sensors. However, this polymorph is only stable between 729 °C and 825 °C. The δ-Bi_2O_3 phase is usually doped with metal ions to stabilize it at a low temperature, but this induces a significant loss of the ion conductivity.[4] Other studies report on the stabilization of the δ-Bi_2O_3 phase at room temperature in thin films deposited by electrodeposition or at high temperatures by chemical vapour/solution deposition,[5] reactive sputtering and carbothermal evaporation. Interfacial stresses and/or the nanocrystalline character of these films are speculated to be possible causes for stabilization of the phase.[6]

Among all bismuth-containing materials, multi-metallic bismuth(III) oxides are probably most interesting for applications in electronics due to their physical properties (*e.g.* ferroelectric, electro-optic or multiferroic). These properties are related to the high polarizability and the distortions induced by the electronic and/or steric effect of the 6s lone pair of Bi^{3+}. This electronic configuration facilitates the hybridization of the 6s orbital of bismuth and the orbitals of other atoms, such as the

[a]Instituto de Ciencia de Materiales de Madrid (ICMM), C.S.I.C., Cantoblanco, E-28049 Madrid, Spain. E-mail: lcalzada@icmm.csic.es; Fax: +34 91 372 0623; Tel: +34 91 334 9000

[b]Departamento de Química y Edafología, Facultad de Ciencias, Universidad de Navarra, E-31008 Navarra, Spain

[c]Hasselt University, Institute for Materials Research, Inorganic and Physical Chemistry, IMEC vzw, Division IMOMEC, B-3590 Diepenbeek, Belgium

† Electronic supplementary information (ESI) available. See DOI: 10.1039/c4tc00960f

2p one of oxygen, inducing the distortion of the unit cell and affecting its properties.[7] The former is the case for the family of bismuth-containing perovskites.[8]

The development of less hazardous compounds is considered a crucial challenge nowadays, especially in the electronic industry, where legislations enforce alternative non-hazardous materials.[9] Bismuth compounds are promising candidates due to the low toxicity of the bismuth metalloid compared with other heavy metals (*e.g.* Pb, Cd or Hg). Therefore, and in the particular case of ferroelectrics, relaxor-ferroelectrics and piezoelectrics, strong efforts are directed on looking for lead-free alternatives for the commercially used lead zirconate titanate, $Pb(Zr_x, Ti_{1-x})O_3$ (PZT). Bismuth-perovskites, such as those based on the multiferroic bismuth ferrite, $BiFeO_3$, or the relaxor-ferroelectric bismuth and sodium titanate, $(Bi_{0.5}Na_{0.5})TiO_3$, are shown as promising candidates in this area.[10] Limitations for these compounds are related to the high annealing temperatures necessary for the crystallization of these perovskite phases.

Consequently, novel synthetic methods that reduce the formation temperature of the oxide would be required for the fabrication of bismuth-based electronic thin films. This is reinforced nowadays by the need for the integration of these materials with substrates of low thermal stability within micro- and flexible-electronic devices.[11]

Recent developments on the low-temperature fabrication of oxide thin films apply UV irradiation onto light-sensitive sol(ution)–gel precursors.[11,12] Energy provided by UV-light hence turns into a powerful tool for the synthesis of inorganic compounds far from their equilibrium conditions: energetic photons produce electronic excitations in bonds, resulting in the dissociation of ligand–metal[13] bonds in the metal–organic or metal–alkoxide compounds, and thus induce the subsequent formation of a metal–O–metal skeleton for the oxide material.

Charge transfer excited states play an important role in the photo-physics and photo-chemistry of metal coordination complexes.[14,15] Metal complexes of d^{10} cations, such as Bi(III), are characterized by reactive metal-to-ligand charge transfer states, where a shift of the electronic distribution can be induced by UV light. Therefore, photo-reactions of these metal complexes could be used within synthesis methods for inorganic materials difficult to obtain otherwise. The design and synthesis of UV-absorber metal complexes turn out to be a key issue to synthesize metal oxide phases.

Alkanolamines are flexible co-ligands that can bind to a large range of metals.[16] Coordination occurs through N-donors and O or OH groups, and can lead to two types of molecules; simple compounds, where the hydroxyl groups of the alkanolamine are bonded to the metal cation, and cyclic compounds, where both the hydroxylic and the amino groups are bonded to the metal. The bond between the nitrogen and the metallic centre incorporates new functionalities into these types of molecules, such as photosensitivity.[14,16]

A metal complex between Bi(III) and an alkanolamine, *N*-methyldiethanolamine, is formed in solution and studied in this work. This complex presents primary bonds, Bi–O, Bi–N, and longer Bi–O-bonds, which can lead to the association of the monomer units. This coordination compound absorbs light in the UV range, promoting the rupture of the organic bonds and the formation of a metal–O–metal skeleton that is the basis for the oxide material. As a result, oxides that cannot be obtained by traditional thermal processing methods can be prepared by this way at low temperatures. The efficiency of this synthesis strategy is demonstrated by the crystallization at 350 °C and the stabilization at room temperature of films of the high-temperature δ-Bi_2O_3 phase. Additionally, the effectiveness of the method is proven by the low temperature (400 °C) preparation of much more challenging complex bismuth based functional oxides: the multiferroic bismuth ferrite, $BiFeO_3$, and the relaxor-ferroelectric bismuth, sodium and barium titanate, $(Bi_{0.5}Na_{0.5})_{0.945}Ba_{0.055}TiO_3$.

2. Experimental section

Synthesis of bismuth-based oxide precursor solutions/sols

Solutions of Bi(III), with and without *N*-methyldiethanolamine ($CH_3N(CH_2CH_2OH)_2$, Aldrich, 99%), hereafter called mdea, were prepared as described in the ESI, Fig. S1–S3.† A bismuth solution (~0.15 mol L^{-1}) was obtained by dissolving bismuth(III) nitrate penta-hydrate ($Bi(NO_3)_3 \cdot 5H_2O$, Aldrich, 99.99%) in 1,3-propanediol ($HO(CH_2)_3OH$, Aldrich, 98%) and acetic acid (CH_3COOH, Merck, 100%) for 24 hours in air using a 1.0 : 4.0 propanediol–acetic acid molar ratio. A transparent solution of Bi(III) was obtained (Fig. S1†). A Bi(III)–mdea solution (~0.15 mol L^{-1}) was prepared by refluxing bismuth(III) nitrate penta-hydrate in 1,3-propanediol, acetic acid and mdea (1.0 : 4.0 diol–acetic acid and 1.0 : 5.0 Bi(III)–mdea molar ratios) for 5 hours in air, resulting in a brown-colored sol (Fig. S1†).

Precursor solutions and sols of bismuth-based multi-oxides, $BiFeO_3$, and $(Bi_{0.5}Na_{0.5})_{0.945}Ba_{0.055}TiO_3$ (ref. 17) were prepared with and without mdea.

The $BiFeO_3$ precursor solution (BFO) was prepared by mixing bismuth(III) nitrate penta-hydrate and iron(III) 2,4-pentanedionate ($Fe(C_5H_8O_3)_3$, Sigma-Aldrich, 99.9%) in acetic acid and 1,3-propanediol (molar ratio acid–diol was 4.0 : 1.0). A dark red colored solution was obtained (~0.25 mol L^{-1}) (Fig. S2†). The $BiFeO_3$–mdea (BFO–mdea) solution was synthesized by mixing a Bi(III)–mdea solution, prepared by following the synthesis procedure described previously, an iron(III) 2,4-pentanedionate solution in acetic acid and 1,3-propanediol (molar ratios of acetic acid–diol 4.0 : 1.0 and of mdea–Bi(III) 5.0 : 1.0). A dark orange colored solution with a concentration of ~0.25 mol L^{-1} was obtained (Fig. S2†).

$(Bi_{0.5}Na_{0.5})_{0.945}Ba_{0.055}TiO_3$ sols with and without mdea, hereafter called BNBT–mdea and BNBT sols, respectively, were synthesized by a hybrid route.[17] Firstly, a precursor sol of $(Bi_{0.5}Na_{0.5})TiO_3$ (BNT) was synthesized by refluxing sodium acetate hydrated ($Na(OCOCH_3) \cdot 3H_2O$, Aldrich, 99%), bismuth acetate ($Bi(OCOCH_3)_3$, Aldrich, 99.99%), and titanium di-isopropoxide bis-acetylacetonate ($Ti(OC_3H_7)_2(CH_3COCHCOCH_3)_2$, Aldrich, 75%) in a mixture of 1,3-propanediol, acetic acid and water in air for 8 hours. The molar ratio of Ti(IV) to any of the solvents was 1.0 : 10.0 and the Ti(IV)–Na(I)–Bi(III) molar ratio of the metal reagents was 2.0 : 1.0 : 1.0. Distilling off byproducts in

a volume of liquid equivalent to 80 vol% of 2-propanol contained in the sol led to an orange precursor sol of $(Bi_{0.5}Na_{0.5})TiO_3$ (~0.60 mol L^{-1}) (Fig. S3†). Another precursor sol of $(Bi_{0.5}Na_{0.5})TiO_3$ was prepared in the same way, but adding mdea in a Bi(III)–mdea molar ratio of 1.0 : 10.0, getting a brown-colored solution (~0.50 mol L^{-1}). After that, barium carbonate ($BaCO_3$, Alfa Aesar, 99.997%) was dissolved in propionic acid (CH_3CH_2COOH, Sigma Aldrich, 99%) and propionic anhydride ($CH_3CH_2COOCOCH_2CH_3$, Aldrich, 99%) (volume ratio of acid–anhydride: 7 : 1) at 140 °C for 2 h. Titanium tetra-butoxide ($Ti(O(CH_2)_3CH_3)_4$, Aldrich, 99%) and 2,4-pentadione ($C_5H_8O_2$, Aldrich, 99%) were added to the Ba(II) solution. Finally, the mixture was diluted with 1-butanol ($C_4H_{10}O$, Sigma-Aldrich, 99.4%) (Fig. S3†).

To obtain gels, the solutions or sols were dried in air, in an oven at 120 °C for 24 h.

Techniques of analysis of the precursors

^1H and ^{13}C Nuclear Magnetic Resonance (NMR) spectra were recorded on the Bi(III) and Bi(III)–mdea solutions with a Bruker Advance 400 MHz (B_o 9.4 T), using a zg30 Bruker pulse program and a delay time between pulses (D_o) of 1 s. Deuterated chloroform ($CDCl_3$) was used as a solvent.

Electro Spray Ionization Mass Spectrometry (ESI-MS) was performed using an AB Sicex Qstar time-of-flight (TOF) MS (mass range ~6000 Da; resolution 9000 FWHM). A diluted Bi(III)–mdea solution (~20 ppm) in acetonitrile (C_2H_3N) was infused into the mass spectrometer with a syringe pump at a flow rate of 20 μL min^{-1}. The mass spectrometry was performed in the positive-ion mode with an ESI source voltage of +5.5 kV.

The thermal decomposition pathways of Bi(III) and Bi(III)–mdea dried gels were studied by means of complementary thermogravimetrical techniques. Conventional thermogravimetric analysis (TGA) was carried out using a TA Instruments SDT Q600 for simultaneous TGA and differential thermal analysis (DTA). TGA-MS measurements were carried out using the TGA equipment (TA Instruments TGA Q5000) coupled with a Pfeiffer Vacuum Thermostar MS. This coupling allows the analysis of the evolved gases during the heating of the gels (TGA-EGA). The MS was set to scan in the m/z = 10–110 range. All thermogravimetric experiments were performed on the dried gels, heated from room temperature to 900 °C (10 °C min^{-1}) in dry air (100 mL min^{-1}).

UV-Vis spectroscopy of the sols and solutions was performed using a Biochrom Libra S35 spectrophotometer. For this, the Bi(III) and Bi(III)–mdea solutions were diluted (10^{-6} mol L^{-1}) with water in order to obtain a reasonable absorbance.

Layers of the Bi(III)–mdea sol were spin-coated (3000 rpm for 45 s) on 2 × 2 cm^2 sized silicon doubled side polishing and fused silica substrates, with the aim of carrying out Fourier transform infrared (FTIR) and UV-Vis spectrometry analysis, respectively. The layers were dried at 150 °C for 10 min. Then, they were heated at 250 °C in an O_2 atmosphere, with or without UV-irradiation for times between 1 min and 60 min. For the UV-irradiation, an excimer lamp (Heraeus-Noblelight Bluelight Curing Module) with $\lambda_{emission}$ = 222 nm, an electrical power of 1.5 kW, a frequency of 50 Hz, an irradiation length of 30 cm and an irradiance of 6.25 W cm^{-2} was used. Samples were placed in a closed chamber, containing a small furnace for the heating of the samples. The temperature of the sample was controlled by an internal and an external thermocouple. This chamber has a top quartz window transparent to the UV-light. In this setup, the distance of the sample to the UV-lamp is 9 cm.

Thin film fabrication and characterization

Crystalline thin films were prepared using the Bi(III), Bi(III)–mdea, BFO–mdea and BNBT–mdea precursor solutions and sols. These liquid precursors were spin-coated on substrates at 3000 rpm for 45 s. Then, the deposited layers were dried at 150 °C for 10 min. The resulting amorphous layers were treated in oxygen at 250 °C for 1 h with or without UV irradiation, using the excimer lamp and the equipment described above. Crystallization of the films was carried out in a rapid thermal processor (RTP, JetStar 100 JIPELEC equipment) at 350 °C (Bi_2O_3 thin films) or at 400 °C (BFO and BNBT thin films) for 1 h in an oxygen atmosphere for the Bi_2O_3 and BNBT films or in air for the BFO films. A heating rate of ~30 °C s^{-1} was used. Drying, irradiation and thermal annealing were repeated for each of the 3 deposited layers. Films were labelled with the same names as their corresponding precursor solutions. The films were prepared on three different substrates: $Pt/TiO_2/SiO_2/(100)Si$, $SiO_2/(100)Si$ and borosilicate glass.

The crystalline phase in the films was monitored by X-ray diffraction (XRD) using a powder diffractometer (D8 Bruker) with a Cu anode (λ = 1.54 Å).

The cross-section and plan-view micrographs of the crystalline oxide films were obtained by field-emission gun scanning electron microscopy (FEG-SEM, Nova Nanosem 230 FEI Company equipment, Hillsboro, OR).

Energy Dispersive X-Ray (EDX) analysis of the multi-metallic oxide thin films was performed with a FEI Nova NanoSEM 230 microscope, equipped with an EDX detector (EDAX Genesis XM2i, resolution 133 eV). This study was carried out on the surfaces of the thin film samples, in a minimum of three different zones with an area of analysis of 10^3 μm^2. Acceleration voltages of 14.5 kV and 10.0 kV were used for the $BiFeO_3$ film and the $(Bi_{0.5}Na_{0.5})_{0.945}Ba_{0.055}TiO_3$ film, respectively.

Capacitors for the electrical characterization were fabricated by sputtering (BAL-TEC SCD 050) platinum on the surface of the crystalline films, using a shadow mask. The functional response was tested by measuring ferroelectric hysteresis loops in a virtual ground set up circuit and a HP 8116A pulse generator. A sinusoidal electric excitation wave of 1 kHz frequency and a maximum amplitude of 15 V was applied. The density of current *versus* applied electric field (*J–E*) curves was measured for the $(Bi_{0.5}Na_{0.5})_{0.945}Ba_{0.055}TiO_3$ and $BiFeO_3$ thin films on Pt-coated Si substrates. From these curves, the compensated ferroelectric hysteresis loops (polarization *versus* applied electric field, *P–E*) were calculated.

3. Results

The synthesis of a photosensitive metal complex of Bi(III) and *N*-methyldiethanolamine ($CH_3N(CH_2CH_2OH)_2$, mdea) was

obtained by refluxing bismuth nitrate penta-hydrate and mdea in 1,3-propanediol and acetic acid. The resulting liquid precursor is denoted as Bi(III)–mdea. This precursor is studied in comparison with the bismuth solution prepared by dissolving bismuth nitrate penta-hydrate in 1,3-propanediol and acetic acid, and this solution is denoted as Bi(III).

NMR spectra of the Bi(III) and Bi(III)–mdea solutions are shown in Fig. 1 and 2, respectively. Only chemical shifts that can be assigned to the protons of the acetic acid ($\delta_{Ha} \sim 1.87$ ppm and $\delta_{Hb} \sim 8.58$ ppm) and 1,3-propanediol ($\delta_{He} \sim 1.78$ ppm, $\delta_{Hc} \sim 1.85$ ppm and $\delta_{Hd} \sim 3.54$ ppm/3.96 ppm) solvents are recorded in the ^{1}H-NMR spectrum of the Bi(III) solution (Fig. 1a). The ^{13}C-NMR spectrum of this solution also shows shifts at $\delta_{Ca} \sim 20.61$ ppm and $\delta_{Cb} \sim 172.29$ ppm/173.82 ppm, confirming the presence of these solvents (Fig. 1b).

The chemical shifts corresponding to acetic acid in the Bi(III)–mdea solution are observed in the ^{1}H-NMR spectrum (Fig. 2a) at $\delta_{Ha} \sim 1.67$ ppm, $\delta_{Hc} \sim 1.60$ ppm and $\delta_{Hd} \sim 3.74$ ppm, close to those recorded in the spectrum of the Bi(III) solution shown in Fig. 1a. In addition, new chemical shifts are detected

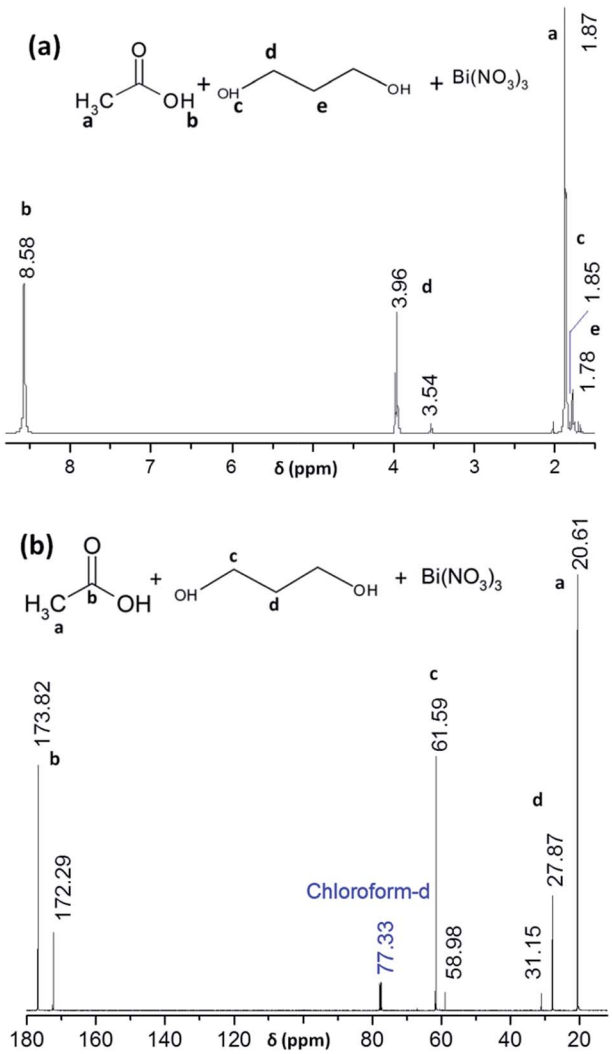

Fig. 1 (a) ^{1}H-NMR and (b) ^{13}C-NMR spectra of the Bi(III) solution.

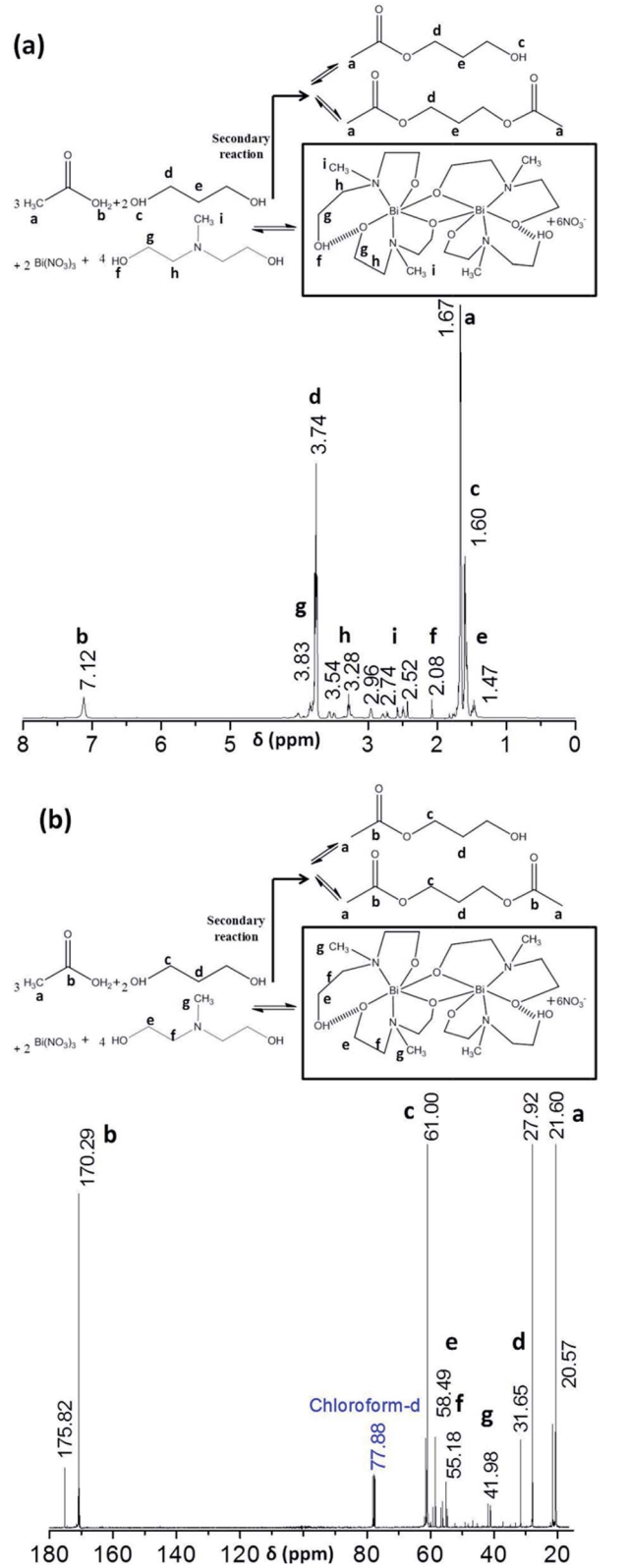

Fig. 2 (a) ^{1}H-NMR and (b) ^{13}C-NMR spectra of the Bi(III)–mdea sol. Insets correspond to the reaction produced during the synthesis of the precursor sol to form the Bi(III)–mdea complex as the product of reaction and esters and di-esters as byproducts.

in the ^{1}H-NMR spectrum of Bi(III)–mdea that appear as multiplets at $\delta_{Hf} \sim 2.08$ ppm, $\delta_{Hi} \sim 2.52$ ppm/2.74 ppm/2.96 ppm, $\delta_{Hh} \sim 3.28$ ppm/3.54 ppm, and $\delta_{Hg} \sim 3.83$ ppm (Fig. 2a). These shifts are assigned to the protons of the mdea ligands.

The ^{13}C-NMR spectrum of the Bi(III)–mdea solution is shown in Fig. 2b. The chemical shifts of the carbons ascribed to acetic acid are close to those for the Bi(III) solution. Note that the signal of the C_b carbon splits into two different shifts at $\delta_{Cb} \sim 170.29$ ppm and 175.82 ppm with a reversed intensity to those recorded in the ^{13}C-NMR spectrum of the Bi(III) solution (Fig. 1b). The signal of C_a also splits into three close shifts at $\delta_{Ca} \sim 20.57/21.60/27.92$ ppm. Signals of the carbons corresponding to 1,3-propanediol are detected as multiplets at $\delta_{Cd} \sim 31.65$ ppm and $\delta_{Cc} \sim 61.00$ ppm. Furthermore, chemical shifts associated with the mdea ligands coordinated to Bi(III) are recorded in the ^{13}C-NMR spectrum. These appear at $\delta C_g \sim 41.98$ ppm, $\delta C_f \sim 55.18$ ppm and $\delta C_e \sim 58.49$ ppm, and are registered as multiplets in the spectrum.

Additional information about the types of ligands and the organic compounds present in these two solutions is extracted from their corresponding infrared (IR) spectra shown in Fig. S4.†

The ESI-MS spectrum (Fig. 3 and S6 in ESI†) of the Bi(III)–mdea sol shows a fragment of $m/z = 445$, which is ascribed to the molecular $[M/2]^+$ ion produced by the fragmentation of the metal complex during the ionization process at +5.5 kV. An additional $[(M/2) + CH_3CN]^+$ ion with $m/z = 484$ is also detected, which is produced by the bounding of the mobile phase (acetonitrile) to the molecular $[M/2]^+$ ion.

The results from the thermogravimetric analysis coupled to mass spectrometry and differential thermal analysis (TGA-MS and DTA) of Bi(III) and Bi(III)–mdea are shown in Fig. 4. The assignment of the most important mass fragments is summarized in Table 1, together with the temperature of the peaks in the TGA-MS curves associated with each of the fragments.[18]

The decomposition process of the dried gels has been divided into three steps (Fig. 4). In the first domain, small weight losses are measured at a temperature of around 50 °C, caused by the volatilization of physically adsorbed solvents; these count for ~1 mass% and ~5 mass% of the Bi(III) and the Bi(III)–mdea gels, respectively. Fragments of $m/z = 17$, 18 and 44 corresponding to HO^+, $H_2O^{+\bullet}$ and CO_2^+, respectively, are recorded around this temperature. Large weight losses associated with high exothermic peaks at 265 °C and 314 °C are detected between 200 °C and 400 °C. Here, notable differences

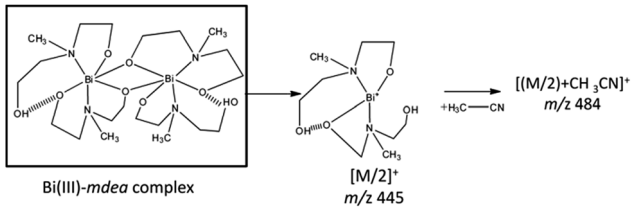

Fig. 3 Mass spectral fragmentations of the Bi(III)–mdea complex detected in the ESI-MS spectrum ($[M/2]^+$, $m/z = 445$ and $[(M/2) + CH_3CN]^+$, $m/z = 484$).

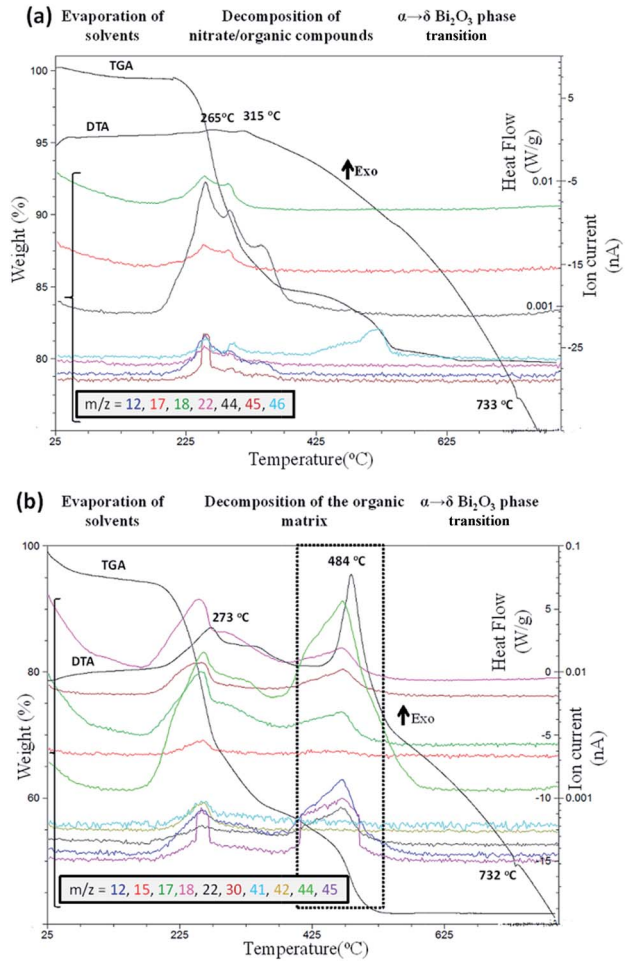

Fig. 4 DTA/TGA-MS profiles of (a) Bi(III) and (b) Bi(III)–mdea dried gels, carried out in dry air (10 °C min^{-1}). Only relevant fragments in the m/z = 5–80 region are shown (ion current).

in weight losses are observed between both systems; ~15% and ~32% for the Bi(III) and Bi(III)–mdea systems, respectively.

The mass fragments detected in this step indicate the decomposition of 1,3-propanediol (m/z = 12, 17, 18) and acetate/carbonate groups (m/z = 12, 17, 18, 22, 44, 45). Weight losses of ~4% for Bi(III) and ~18% for Bi(III)–mdea are detected between 400 °C and 600 °C. A characteristic m/z fragment ascribed to the decomposition of methyl-amines ($m/z = 41$) is observed for Bi(III)–mdea in this temperature interval, whereas a m/z fragment of 46 is detected for Bi(III), associated with the NO_2^+ ion, coming from the starting reagent. At temperatures over 600 °C, an endothermic peak around 730 °C is recorded in the DTA curves for both systems. This endothermic process, without any appreciable weight loss or released fragment, has been associated with the α → δ phase transition of the Bi_2O_3 oxide.[1,19]

The UV spectra of the Bi(III) and Bi(III)–mdea solutions are shown in Fig. 5. The high absorption recorded in both spectra at ~200 nm is ascribed to the cut-off wavelength. The absorption maximum at ~250 nm[12] in the Bi(III)–mdea solution is neither observed for Bi(III) nor for pure free *N*-methyldiethanolamine

Table 1 Peak assignment and occurrence of mass fragments in the TGA-MS profile of the Bi(III) and Bi(III)–mdea dried gels

m/z	Fragments (ions) that result during the thermal decomposition of the precursors	Temperatures (°C) of the peaks in the TGA-MS curves at which the different fragments are eliminated from the system	
		Bi(III) solution	Bi(III)–mdea sol
12	C^+	253, 289, 344	260, 450
15	CH_3^+		250
17	OH^+	253, 295	250
18	H_2O^+	253, 295	250, 470
22	CO_2^{2+}	253	250, 470
30	$CH_2NH_2^+$		250, 470
41	$C_2H_3N^+$		260
42	$C_2H_2O^+$		260
44	CO_2	253, 295, 340	260, 470
45	CHO_2^+, $C_2H_5O^+$, CO_2H^+, $^{13}CO_2^+$	254	256, 470
46	NO_2^+	253, 295	

(mdea) (Fig. S7†). In the Bi(III) solution, a shoulder between 240 nm and 260 nm is detected, which is ascribed to the n → π* transition of the C=O group of the acetic acid solvent.[18]

The FTIR and UV spectra of the UV-irradiated and non-irradiated Bi(III)–mdea films are shown in Fig. 6. The FTIR spectrum of the initial film (0 minutes) (Fig. 6a) presents an band at ~3400 cm^{-1}, ascribed to the ν(O–H) stretching vibrations of the OH groups of mdea, esters as byproducts of the reaction[18] and residual solvent molecules trapped in the dried film (see the reaction scheme inserted in Fig. 2). The bands at ~2960 cm^{-1}, ~2900 cm^{-1} and ~2860 cm^{-1} are due to ν(C–H) stretching vibrations. These are ascribed to three different C–H groups.[18] (i) The ν(C–H) at ~2960 cm^{-1} corresponds to C–H groups close to O-(denoted as $\nu(C–H)_O$), which are in the trapped solvents and mdea. (ii) The ν(C–H) at ~2900 cm^{-1} is produced by those C–H groups closest to the carbonyl groups (denoted as $\nu(C–H)_{CO}$). These are mainly present in the byproducts (esters and diesters) (Fig. S5 and Table SI†). Finally, (iii) the ν(C–H) at ~2860 cm^{-1} is due to the C–H groups next to N-(denoted as $\nu(C–H)_N$). They are present in the mdea ligand. The bands at ~1730 cm^{-1}, ~1630 cm^{-1} and ~1550 cm^{-1} are associated with the ν(C=O), $\nu(CO_2)_a$ and $\nu(CO_2)_s$ stretching vibrations of the carboxyl groups of the ester/diester. After 1 minute of heating at 250 °C, with or without UV-irradiation, the $\nu(C–H)_{CO}$ at ~2900 cm^{-1} and ν(CO) at ~1730 cm^{-1} bands, related to the byproducts, have almost disappeared. Upon irradiation, the ν(O–H) at ~3400 cm^{-1}, $\nu(C–H)_O$ at ~2960 cm^{-1} and $\nu(C–H)_N$ at ~2860 cm^{-1}, due to the Bi(III)–mdea complex, decrease exponentially in intensity (the inset of Fig. 6a). They practically disappear after 10 minutes of UV-irradiation. However, for the non-irradiated films, the decrease of the intensity of these stretching vibrations is significantly lower, not observing them after 60 minutes of heating (the inset of Fig. 6a).

The UV spectra (Fig. 6b) indicate a similar behavior to that observed in the FTIR study. A large decrease in the absorption of the UV-irradiated films for λ < 225 nm is observed after 1 minute of irradiation, which is not observed in the non-irradiated films. This absorption region corresponds to n → σ* and n → π* electronic transitions in C–N (from mdea) and C=O (from esters and diesters byproducts) chromophore groups.[18] After 10 minutes of UV-irradiation, the shape of the absorption curve of the UV-irradiated films has changed, observing the disappearance of the absorption maximum at ~250 nm, associated with MLCT transitions of the Bi(III)–mdea complex. This does not occur in the non-irradiated films until 60 minutes of heating. The shape of this curve (after 60 minutes of heating for the non-irradiated films and 10 minutes of heating for the UV-irradiated films) is the same as that of Bi_2O_3 films crystallized at 350 °C (Fig. S9†).

Both Bi(III) and Bi(III)–mdea precursors are used for the chemical solution deposition (CSD) of bismuth based electronic oxide thin films. The effect of UV-irradiation on promoting the advancement in the formation of crystalline oxide films at low temperature is studied.

X-ray diffraction patterns of the Bi(III) or Bi(III)–mdea films, prepared with/without UV irradiation, thermally treated at 250 °C or 350 °C and deposited on different substrates, are shown in Fig. S12.† These results indicate that, as expected, the low-temperature phases of bismuth(III) oxide, monoclinic α-Bi_2O_3 or the *meta*-stable orthorhombic ε-Bi_2O_3 low-temperature phases are obtained for all films, with the exception of the Bi(III)–mdea film excited with UV-light and annealed at 350 °C.

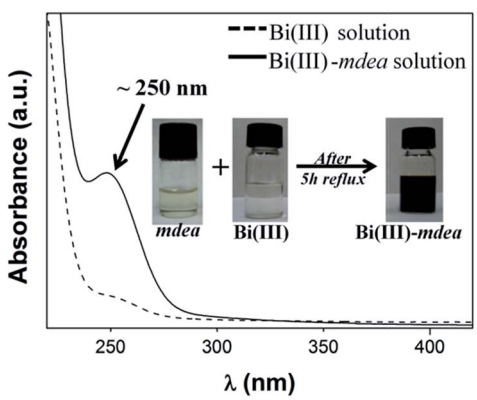

Fig. 5 UV spectra of the Bi(III) and Bi(III)–mdea solutions.

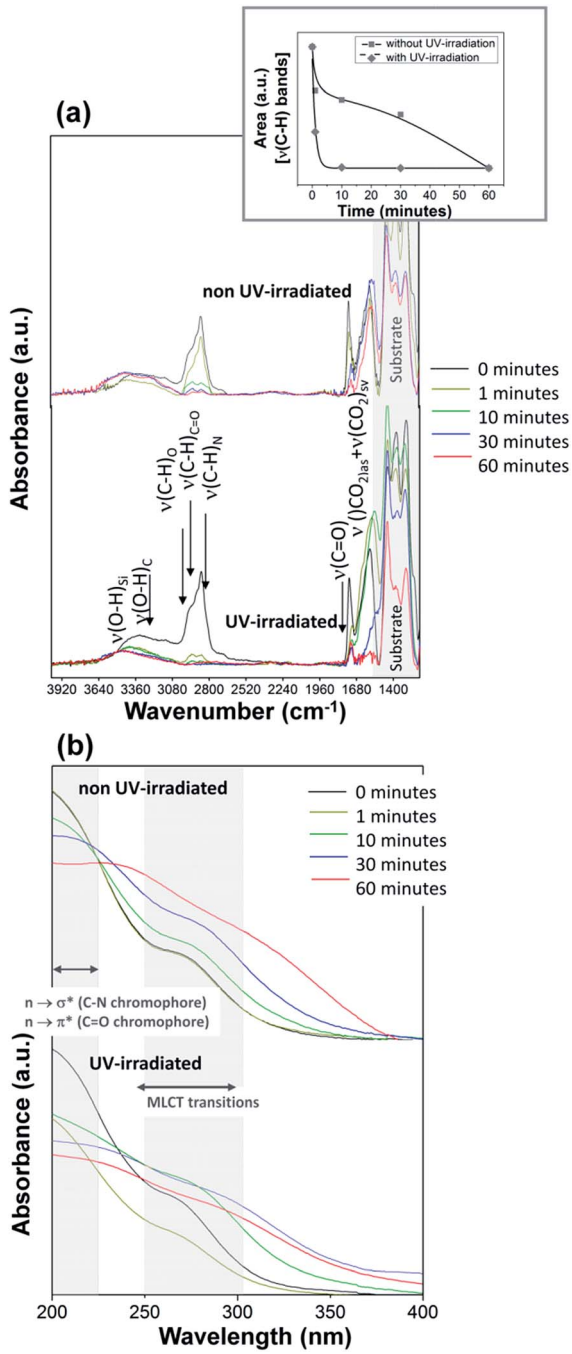

Fig. 6 (a) FTIR and (b) UV spectra of the Bi(III)–mdea films treated at 250 °C in O_2 for 0, 1, 10, 30 and 60 minutes, without UV-irradiation and with UV-irradiation during heating. (a) FTIR spectra were measured for films deposited on the silicon doubled side polishing substrate and in the wavelength region from 4000 cm^{-1} to 1200 cm^{-1}. The inset shows the decrease of the integrated area of the ν(C–H) bands as a function of heating time. (b) UV spectra were measured for films deposited on fused silica substrates, in the wavelength region from 200 to 400 nm.

In the latter, the high-temperature δ-Bi_2O_3 phase is formed at only 350 °C and is stable at room temperature (Fig. 7a). This phase shows a {111} preferred orientation, independent of the type of substrate, either amorphous or single-crystals. The SEM micrograph (Fig. 7b) of the δ-Bi_2O_3 film on a silicon substrate reveals the formation at 350 °C of a crystalline film with a dense and uniform microstructure, and with a thickness of ~120 nm.

The photosensitive Bi(III)–mdea metal complex here synthesized was investigated, in addition, as a bismuth source for the fabrication of functional Bi-based perovskite thin films. Multi-metallic oxide thin films are prepared; bismuth ferrite ($BiFeO_3$) and bismuth, sodium and barium titanate $(Bi_{0.5}Na_{0.5})_{0.945}Ba_{0.055}TiO_3$. They are deposited on Pt-coated substrates. Fig. 8a and b show the X-ray diffraction patterns of these oxide films prepared by UV-irradiation and annealing at 400 °C. A perovskite phase is formed in both films; $BiFeO_3$ (JCPDS-ICDD 86-1518 file)[17,20] and $(Bi_{0.5}Na_{0.5})_{0.945}Ba_{0.055}TiO_3$.[17,21] Significant peaks associated with secondary crystalline phases are not detected.

The SEM cross-section images of the $BiFeO_3$ and $(Bi_{0.5}Na_{0.5})_{0.945}Ba_{0.055}TiO_3$ thin films are shown in Fig. 8c and d. These films have a thickness of ~110 nm and ~335 nm, respectively. The large thickness and the small grain size of the $(Bi_{0.5}Na_{0.5})_{0.945}Ba_{0.055}TiO_3$ films reveal the lack of sintering in the bulk film. According to the EDX analysis (Fig. S13 in ESI†), the experimental Bi/Fe atomic ratio is 1.10 ± 0.10 for the $BiFeO_3$ film, which is close to the theoretical value of 1.00. For the $(Bi_{0.5}Na_{0.5})_{0.945}Ba_{0.055}TiO_3$ film, the experimental Bi/Ti atomic ratio is 0.49 ± 0.10, in accordance with the theoretical solid solution atomic ratio of Bi/Ti = 0.47. This indicates that for such complex oxide films, the crystallization of the perovskite

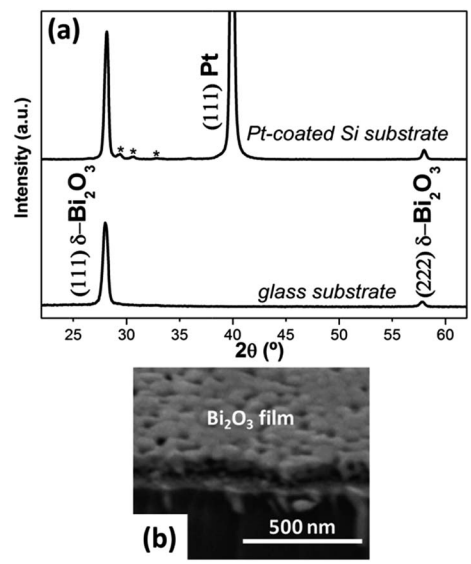

Fig. 7 (a) X-ray diffraction patterns of UV-irradiated bismuth oxide films derived from the Bi(III)–mdea solution and thermally treated at 350 °C. Peaks are indexed according to the δ-Bi_2O_3 phase (JCPDS-ICDD file 27-0052). The films are deposited on an amorphous glass substrate and a (111)Pt/TiO_2/SiO_2/(100)Si substrate. The Pt peaks are indexed to the JCPDS-ICDD file 4-0802, and * indicates other polymorphic forms of Bi_2O_3. Additional information on the different bismuth oxide phases obtained in films derived from the Bi(III) or Bi(III)–mdea solutions, with/without UV-irradiation, annealed at low temperatures and on different substrates, is shown in Fig. S11.† (b) SEM image of the δ-Bi_2O_3 film on a silicon substrate.

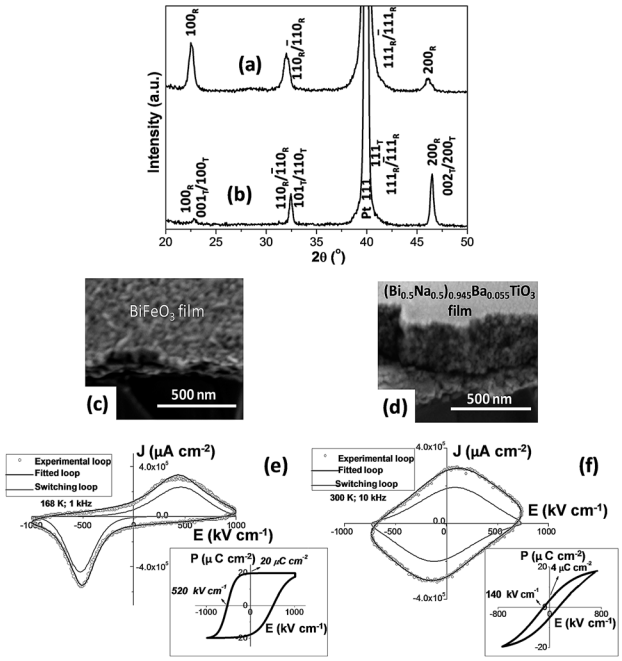

Fig. 8 X-ray diffraction patterns of the (a) $BiFeO_3$ and (b) $(Bi_{0.5}Na_{0.5})_{0.945}Ba_{0.055}TiO_3$ films. Reflections corresponding to both perovskite phases, $BiFeO_3$ and $(Bi_{0.5}Na_{0.5})_{0.945}Ba_{0.055}TiO_3$, are indexed to each pattern.[17,20,21] SEM cross-section micrographs of the (c) $BiFeO_3$ and (d) $(Bi_{0.5}Na_{0.5})_{0.945}Ba_{0.055}TiO_3$ films. *J–E* hysteresis loops of the (e) $BiFeO_3$ and (f) $(Bi_{0.5}Na_{0.5})_{0.945}Ba_{0.055}TiO_3$ films, measured at 168 K and 1 kHz and 300 K and 10 kHz, respectively. Insets of (e) and (f) show *P–E* compensated hysteresis loops calculated from the *J–E* curves.

phase with the stoichiometric oxide composition can be achieved at a low temperature by the method proposed.

The functionality of these low-temperature processed films is demonstrated by measuring their ferroelectric response (Fig. 8e and f and Section 11 of the ESI†). *J–E* curves were measured for both films and from them, the compensated ferroelectric hysteresis loops[22] were calculated (insets of Fig. 8e and f). For the $BiFeO_3$ film a P_r of ~40 μC cm^{-2} and an E_c of ~ 520 kV cm^{-1} were obtained. For this film, measurements were carried out at 168 K to minimize leakage currents and conductivities.[17] For the $(Bi_{0.5}Na_{0.5})_{0.945}Ba_{0.055}TiO_3$ film, a remnant polarization of $P_r \sim 8$ μC cm^{-2} and a coercive field of E_c ~ 140 kV cm^{-1} were obtained at 300 K. The low remanence of the loop of this film (the inset of Fig. 8f) is a characteristic for these types of relaxor-ferroelectric compounds, with losses and unstable ferroelectric domains.[23]

To realize the considerable reduction obtained in the crystallization temperature of these functional complex oxide thin films, note that the lower limit temperature to obtain $(Bi_{0.5}Na_{0.5})_{0.945}Ba_{0.055}TiO_3$ films with ferroelectric properties reported in the literature is over 600 °C.[10,17,23]

The thermal decomposition pathway (DTA/TGA-MS analysis) and the efficiency of the UV-irradiation to get a prompt elimination of the organic compounds in the precursors containing the Bi(III)–mdea metal complex are shown for the $(Bi_{0.5}Na_{0.5})_{0.945}Ba_{0.055}TiO_3$ powders and films in Fig. S10 and S11.†

4. Discussion

The synthesis of a bismuth oxide precursor, based on coordination complexes with *N*-methyldiethanolamine (mdea) is proven here by the results shown in Fig. 1–4.

The formation of a bismuth complex in the Bi(III)–mdea sol is confirmed by the ^{1}H-NMR and ^{13}C-NMR spectra shown in Fig. 2. The chemical shifts corresponding to carbons and protons belonging to mdea (C_e, C_f, C_g and H_g, H_h, H_i) are recorded as multiplets in these spectra. These splitted signals, associated with sterically non-equivalent mdea groups, can be explained by the coordination of mdea to bismuth and the formation of a dimeric metal complex, as proposed by Le Bris *et al.*[24] In addition, the NMR spectra reveal the existence of esters and di-esters in the Bi(III)–mdea sol, which result from the reaction between the solvents, acetic acid and 1,3-propanediol, during synthesis. This can be deduced from the higher intensity of the signal at ~170.73 ppm, ascribed to the C_b atoms of the ester/di-ester, compared to that at ~175.20 ppm, due to the C_b atoms of the acetic acid (Fig. 2b). In contrast, the ^{13}C-NMR spectrum of the Bi(III) solution shows a higher intensity for the shift ascribed to the C_b atoms of acetic acid at ~173.82 ppm (Fig. 1b). The low intensity of the H_b signals in the^{1}H-NMR spectrum of the Bi(III)–mdea solution (Fig. 2a), compared to those of the spectrum of the Bi(III) sol (Fig. 1a), could be due to a reduction of the number of chemically equivalent protons in the former, as a consequence of the ester/di-ester formation (Fig. S5 and Table, ESI†). This reaction ensures the formation of a Bi(III)–mdea complex, inhibiting the reaction between bismuth and diol, since dihydroxy-alcohols are reported to work as mono- or bi-dentate ligands with some metal ions.[25,26]

The ESI-MS results shown in Section 4 of ESI† support the molecular structure proposed for the Bi(III)–mdea complex shown in Fig. 3. In addition, the DTA/TGA-MS profiles corroborate the formation of the Bi(III)–mdea complex. Fig. 4 shows important differences between the decomposition processes of the Bi(III) and the Bi(III)–mdea gels. For the Bi(III) gel, several chemical processes are occurring in the 200 °C–400 °C region. Here, the organic compounds in the gel matrix partially decompose, which is apparent from characteristic fragments of primary alcohols and carboxylic acids, such as OH^+, $H_2O^{+\bullet}$, CO_2^+ and $CO_2H^{+\bullet}$. The dehydration of bismuth nitrate penta-hydrate is also detected in this temperature interval (from 200 °C to 400 °C),[27] which is followed by the subsequent decomposition of $Bi(NO_3)_3$ and the formation of Bi_2O_3 at higher temperatures (~575 °C). Thus, a $m/z = 46$ fragment, identified as NO_2^+, is detected in the MS profiles of the Bi(III) precursor. However, this fragment is not recorded in the TGA-MS curves of the Bi(III)–mdea gel, indicating that the bismuth precursor ($Bi(NO_3)_3$) has reacted with the mdea ligands, forming the Bi(III)–mdea complex. Actually, a $C_2H_3N^+$ fragment ($m/z = 41$) is eliminated from this system between 200 °C and 400 °C, which is associated with the decomposition of amines. Therefore, this study supports the formation of a metal complex between Bi(III) and mdea, since the volatilization of a possible non-coordinated *N*-methyldiethanolamine would be detected at temperatures

below 200 °C (Fig. S7†). Besides, the maximum of absorption at $\lambda \sim 250$ nm of the Bi(III)–mdea solution (Fig. 5), supports the formation of this complex.

Based on the aforementioned results, the reaction shown in the inset of Fig. 2 is proposed for the formation of a six-coordinated octahedral complex between Bi(III) and mdea, where mdea acts as a tridentate ligand.[24] Reactions of other cations (*e.g.*, Ti(IV), Pb(II), Al(III), Sn(IV) or B(III)) with alkanolamines have been investigated by other authors, assuming the formation of complexes with a type of structure in which the nitrogen and oxygen atoms coordinate with the cation.[13,16,24,28]

The complex contains Bi(III), a d^{10} element, where ligand field excited states are not possible. Charge transfer (CT) transitions in this complex may occur from a molecular orbital with a predominantly metal-like (M) character to another one with a ligand-like (L) character, exhibiting photoreactivity promoted by MLCT transitions.[13,14] Owing to this, the metal complex here reported is an excellent candidate to enhance the degradation of organics by photolysis after their excitation with electromagnetic radiation of the appropriate wavelength. The monitoring of the photoreaction of this Bi(III)–mdea complex by FTIR and UV spectroscopy (Fig. 6) proves the efficiency of the UV-irradiation to photo-dissociate the metal–ligand bonds of the Bi(III)–mdea precursor. This ultimately leads to an advancement in the formation of the metal–O–metal bonds, the basis of the oxide material.

The UV spectra of Fig. 5 confirm the aforementioned. The absorption maximum at ~250 nm in the Bi(III)–mdea system of the former cannot be ascribed to some of the absorption maxima of free *N*-methyldiethanolamine (mdea)[13] (Fig. S7†). In contrast, it is the characteristic absorption maximum of the coordination complexes of mdea with d^0 or d^{10} metal cations (see, as an example, the UV spectra of Fig. S8† for Zr(IV) and Ba(II)). In addition, the reddish-brown color of the Bi(III)–mdea solution (Fig. 5) indicates the presence of electronic transitions induced by the absorption of Vis-light. As a consequence, UV-irradiation could be able to electronically excite molecular orbitals and thus, induce photolysis of this metal complex.

To evidence the proposed mechanism, thin layers of the Bi(III)–mdea solution are deposited on different substrates and thermally treated at a low temperature (350 °C) after irradiation with the excimer lamp. It is remarkable for the formation of the high-temperature δ-Bi_2O_3 phase instead of the monoclinic α-Bi_2O_3 in the UV irradiated films derived from the Bi(III)–mdea system (Fig. 7). This high-temperature polymorph has been stabilized at room temperature in thin films deposited by different high temperature techniques or by electrodeposition.[5] The nanocrystalline character of the films and/or interfacial stresses is hypothesized as being responsible for the stabilization of the δ-Bi_2O_3 phase. However, in this work, photoreactions induced by UV-light in the Bi(III)–mdea precursor should be in the origin of the formation and stabilization of this phase at low temperature, since it is not formed in the films deposited from the Bi(III) precursor, with/without UV-irradiation, or from the Bi(III)–mdea without irradiation (Fig. S12†).

The significance of these results is therefore related to the development of a novel synthetic route that enables the reduction of the crystallization temperature of bismuth-based oxides, confirmed here on the high-temperature cubic δ-Bi_2O_3 phase at about 400 °C lower than those temperatures used for conventional processes. Furthermore, the general applicability of this synthesis strategy is demonstrated by the preparation of multi-metallic oxides at low temperature, bismuth based perovskites, such as $BiFeO_3$ or $(Bi_{0.5}Na_{0.5})_{0.945}Ba_{0.055}TiO_3$, with remarkable functionalities proven by their ferroelectric and relaxor-ferroelectric response, respectively (Fig. 8). The master key of this method is the synthesis of a UV-absorber molecule in solution formed between Bi(III) and *N*-methyldiethanolamine (Bi(III)–mdea) (the inset of Fig. 2). The UV-irradiation/excitation of this metal complex is the basis of a novel preparation method, different from the traditional thermal processing of inorganic materials that seems to be highly competitive for the low-temperature crystallization of electronic bismuth-based oxide thin films.

5. Conclusions

A metal complex with charge transfer excited states formed between Bi(III) and *N*-methyldiethanolamine (Bi(III)–mdea) is synthesized in solution as a liquid precursor for the preparation of bismuth-based oxide thin films. The photoreactivity of this metal complex makes the formation of a metal–O–metal oxide skeleton possible in the deposited layer by excitation with UV light. This enables the stabilization and formation by low thermal annealing (350 °C) of the high-temperature cubic δ-Bi_2O_3. The notable decrease of the crystallization temperature of much more complex multi-metallic bismuth-based oxides (multiferroic $BiFeO_3$ and relaxor-ferroelectric $(Bi_{0.5}Na_{0.5})_{0.945}Ba_{0.055}TiO_3$ perovskites) achieved by this process demonstrates the general applicability of this low-temperature solution method. From these results, this processing approach reveals itself as an effective low-temperature synthetic route to access non-equilibrium or high-temperature stable oxide phases that cannot be obtained by traditional thermal processing.

Acknowledgements

This work was financed by the Spanish Project MAT2010-15365 and MAT2013-40489. D. Pérez-Mezcua acknowledges the financial support of the FPU Spanish program (AP2012-0639 Grant). I. Bretos and C. De Dobbelaere are postdoctoral fellows financed by the Juan de la Cierva Spanish Programme and the Fund for Scientific Research of Flanders (FWO), respectively. The authors acknowledge the information provided by Prof. S. Daniele of the University Claude Bernard Lyon – France, on the molecular structure of the metal complex formed between bismuth and *N*-methyldiethanolamine.

References

1 M. Mehring, *Coord. Chem. Rev.*, 2007, **251**, 974.
2 H. T. Fan, S. S. Pan, X. M. Teng, C. Ye, G. H. Li and L. D. Zhang, *Thin Solid Films*, 2006, **513**, 142.

3 H. A. Harwig and G. Gerards, *J. Solid State Chem.*, 1978, **26**, 265.
4 (*a*) A. M. Azad, S. Larose and S. A. Akbar, *J. Mater. Sci.: Mater. Electron.*, 1994, **29**, 4135; (*b*) S. Sarat, N. Sammes and A. Smirnova, *J. Power Sources*, 2006, **160**, 892; (*c*) P. Shuk, H. D. Wiemhöfer, U. Guth, W. Göpel and M. Greenblatt, *Solid State Ionics*, 1996, **89**, 179.
5 (*a*) P. A. Williams, A.-C. Jones, J. C. Crosbie, P. J. Wright, J. F. Bickley, A. Steiner, H. O. Davies, T. J. Leedham and G. W. Critchlow, *Chem. Vap. Deposition*, 2001, **7**, 205; (*b*) S. J. A. Moniz, C. S. Blackman, C. J. Carmalt and G. Hyett, *J. Mater. Chem.*, 2010, **20**, 7881; (*c*) C. Bedoya, G. G. Condorelli, G. Anastasi, A. Baeri, F. Scerra and I. L. Fragala, *Chem. Mater.*, 2004, **16**, 3176; (*d*) S. J. A. Moniz, D. Bhachu, C. S. Blackman, A. J. Cross, S. Elouali, D. Pugh, R. Quesada-Cabrera and S. Vallejos, *Inorg. Chim. Acta*, 2012, **380**, 328.
6 (*a*) E. W. Bohannan, C. C. Jaynes, M. G. Shumsky, J. K. Barton and A. Switzer, *Solid State Ionics*, 2000, **131**, 97; (*b*) J. A. Switzer, M. G. Shumsky and E. W. Bohannan, *Science*, 1999, **284**, 293; (*c*) C. Bedoya, G. G. Condorelli, G. Anastasi, A. Baeri, F. Scerra, I. L. Fragala, J. G. Lisoni and D. Wouters, *Chem. Mater.*, 2004, **16**, 3176; (*d*) A. Helfen, S. Merkourakis, G. Wang, M. G. Walls, E. Roy, K. Yu-Zhang and Y. Leprince-Wang, *Solid State Ionics*, 2005, **176**, 629; (*e*) T. Takeyama, N. Takahashi, T. Nakamura and S. Itoh, *Mater. Lett.*, 2006, **60**, 1733; (*f*) T. Takeyama, N. Takahasy, T. Nakamura and S. Itoh, *Surf. Coat. Technol.*, 2006, **200**, 4797; (*g*) H. T. Fan, S. S. Pan, X. M. Teng, C. Ye, G. H. Li and L. D. Zhang, *Thin Solid Films*, 2006, **513**, 142.
7 (*a*) I. Caracelli, I. Haiduc, J. Zukerman-Schpector and E. R. T. Tiekink, *Coord. Chem. Rev.*, 2013, **257**, 2863; (*b*) R. E. Cohen, *Nature*, 1992, **358**, 136.
8 N. Setter, D. Damjanovic, L. Eng, G. Fox, S. Gevorgian, A. Hong, S. Kingon, H. Kohlstedt, N. Y. Park, G. B. Stephenson, I. Stolitchnov, A. K. Taganstev, D. V. Taylor, T. Yamada and S. Streiffer, *J. Appl. Phys.*, 2006, **100**, 051606.
9 (*a*) EU-DIRECTIVE 2011/65/EU, Restrictions of the use of certain substances in electrical and electronic equipments (RoHS)", Off. J. Eur. Union, 20133, 24[L174], 89; (*b*) International Technologies Roadmap for Semiconductors (ITRS), 2012 Update, http://www.itrs.net/Links/2012ITRS/Home2012.htm.
10 (*a*) Y. Saito, H. Takao, T. Tani, T. Nonoyama, K. Takatori, T. Homma, T. Nagaya and M. Nakamura, *Nature*, 2004, **432**, 84; (*b*) C. Xu, D. Lin and K. W. Kwok, *Solid State Sci.*, 2008, **10**, 934; (*c*) M. D. Maeder, D. Damjanovic and N. Setter, *J. Electroceram.*, 2004, **13**, 385; (*d*) W. Eerenstein, N. D. Mathur and J. F. Scott, *Nature*, 2006, **442**(7104), 759; (*e*) M. Alexe and D. Hesse, *Nat. Commun.*, 2011, **2**, 256; (*f*) S. J. A. Moniz, R. Quesada-Cabrera, C. S. Blackman, J. Tang, P. Southern, P. M. Weaver and C. J. Carmalt, *J. Mater. Chem. A*, 2014, **2**, 2922.
11 (*a*) S. T. Han, Y. Zhou and V. A. L. Roy, *Adv. Mater.*, 2013, **25**(38), 5425; (*b*) I. Bretos, R. Jiménez, A. Wu, A. I. Kingon, P. M. Vilarinho and M. L. Calzada, *Adv. Mater.*, 2014, **26**(9), 1405; (*c*) S. Jeong and J. Moon, *J. Mater. Chem.*, 2012, **22**, 1243.
12 (*a*) M. L. Calzada, I. Bretos, R. Jiménez, H. Guillon and L. Pardo, *Adv. Mater.*, 2004, **16**, 1620; (*b*) M. L. Calzada, A. González, R. Poyato and L. Pardo, *J. Mater. Chem.*, 2003, **13**, 1451; (*c*) C. De Dobbelaere, M. L. Calzada, R. Jiménez, J. Ricote, I. Bretos, J. Mullens, A. Hardy and M. K. Van Bael, *J. Am. Chem. Soc.*, 2011, **133**, 12922.
13 (*a*) N. Martín-Arbella, I. Bretos, R. Jiménez, M. L. Calzada and R. Sirera, *J. Mater. Chem.*, 2011, **21**, 9051; (*b*) I. Imai, in *Hand book of sol–gel science and technology: processing, characterization and applications*, Kluwer Academic, New York, US, 2005.
14 A. Vogler and H. Kunkeley, *Coord. Chem. Rev.*, 1998, **177**, 81.
15 (*a*) S. Trudel, G. Gli, X. Zhang and R. H. Hill, *J. Photopolym. Sci. Technol.*, 2006, **19**, 467; (*b*) S. Trudel, C. H. W. Jones and R. H. Hill, *J. Mater. Chem.*, 2007, **17**, 2206; (*c*) G. E. B. Core, M. Tejosr, A. H. Klann, G. Cabello, A. Lucero and R. H. Hill, *J. Chil. Chem. Soc.*, 2007, **52**(4), 1218; (*d*) R. D. L. Smith, M. S. Prevot, R. D. Fagan, A. Ahang, P. A. Sedach, M. K. J. Siu, S. Trudel and C. P. Berlinguette, *Science*, 2013, **340**, 60; (*e*) H. Park, S. Jung, H. Park, T. S. Kim and R. H. Hill, *Sens. Actuators, B*, 2007, **126**, 289.
16 J. W. Sharples and D. Collison, *Coord. Chem. Rev.*, 2014, **260**, 1.
17 (*a*) C. Gutiérrez-Lázaro, I. Bretos, R. Jiménez, J. Ricote, H. El Hosiny, D. Pérez-Mezcua, R. J. Jiménez Rioboó, M. García-Hernández and M. L. Calzada, *J. Am. Ceram. Soc.*, 2013, **96**, 3061; (*b*) D. Pérez-Mezcua, R. Sirera, I. Bretos, J. Ricote, R. Jiménez, L. Fuentes-Cobas, R. Escobar-Galindo and M. L. Calzada, *J. Am. Ceram. Soc.*, 2014, **97**(4), 1269.
18 (*a*) E. Prestch, P. Bühlmann and M. Badertscher, in *Structural Determination of Organic Compounds*, Springer, Berlin Heidelberg, 2009; (*b*) A. Hardy, K. Van Werde, G. Vanhoyland, M. K. Van Bael, J. Mullens and L. C. Van Pouche, *Thermochim. Acta*, 2003, **397**, 143; (*c*) I. Truijen, A. Hardy, M. K. Van Bael, H. Van den Rul and J. Mullens, *Thermochim. Acta*, 2007, **456**, 38.
19 V. Fruth, M. Popa, D. Berger, C. M. Ionica and M. Jitianu, *J. Eur. Ceram. Soc.*, 2004, **24**, 1295.
20 S. K. Singh, R. Ueno, H. Funakubo, H. Uchida, S. Koda and S. Ishiwara, *Jpn. J. Appl. Phys.*, 2004, **44**(12), 8525.
21 D. Alonso-Sanjose, R. Jiménez, I. Bretos and M. L. Calzada, *J. Am. Ceram. Soc.*, 2009, **92**, 2218.
22 R. Jiménez, C. Alemany, M. L. Calzada, A. González, J. Ricote and J. Mendiola, *Appl. Phys. A*, 2002, **75**, 607.
23 (*a*) A. Perez-Rivero, J. Ricote, I. Bretos, M. L. Calzada, J. L. Pérez de la Cruz, J. R. A. Fernández and R. Jiménez, *J. Am. Ceram. Soc.*, 2014, **97**(4), 1276; (*b*) N. Scarisoreanu, F. Craciun, V. Ion, S. Birjega and M. Dinescu, *Appl. Surf. Sci.*, 2007, **254**, 1292; (*c*) Y. Guo, D. Akai, K. Sawada and M. Ishida, *Solid State Sci.*, 2008, **10**, 928.
24 J. Le Bris, L. G. Hubert-Pfalzgraf, S. Daniele and J. Vaissermann, *Inorg. Chem. Commun.*, 2007, **10**, 80.
25 D. C. Bradley, R. C. Mehrotra, I. P. Rothwell and A. Singh, in *Alkoxo and Aryloxo Derivates of Metals*, Academic Press, California, 2001.

26 (*a*) N. J. Phillips, M. L. Calzada and S. J. Milne, *J. Non-Cryst. Solids*, 1992, **147**, 285; (*b*) M. L. Calzada, R. Sirera, F. Carmona and B. Jiménez, *J. Am. Ceram. Soc.*, 1995, **78**(7), 1802; (*c*) N. J. Phillips, S. J. Milne, N. Ali and J. D. Kennedy, *J. Mater. Sci. Lett.*, 1994, **13**(21), 1535.
27 M. L. Calzada, B. Malic, R. Sirera and M. Kosec, *J. Sol-Gel Sci. Technol.*, 2002, **23**, 221.
28 C. Rat, C. Silvestru and H. Breuning, *Coord. Chem. Rev.*, 2013, **257**, 868.